Meridional Density Gradients Do Not Control the Atlantic Overturning Circulation

AGATHA M. DE BOER

School of Environmental Science, University of East Anglia, Norwich, United Kingdom

ANAND GNANADESIKAN

NOAA/Geophysical Fluid Dynamics Laboratory, Princeton, New Jersey

NEIL R. EDWARDS

Earth and Environmental Sciences, Open University, Milton Keynes, United Kingdom

ANDREW J. WATSON

School of Environmental Science, University of East Anglia, Norwich, United Kingdom

(Manuscript received 17 December 2008, in final form 17 August 2009)

ABSTRACT

A wide body of modeling and theoretical scaling studies support the concept that changes to the Atlantic meridional overturning circulation (AMOC), whether forced by winds or buoyancy fluxes, can be understood in terms of a simple causative relation between the AMOC and an appropriately defined meridional density gradient (MDG). The MDG is supposed to translate directly into a meridional pressure gradient. Here two sets of experiments are performed using a modular ocean model coupled to an energy–moisture balance model in which the positive AMOC–MDG relation breaks down. In the first suite of seven model integrations it is found that increasing winds in the Southern Ocean cause an increase in overturning while the surface density difference between the equator and North Atlantic drops. In the second suite of eight model integrations the equation of state is manipulated so that the density is calculated at the model temperature plus an artificial increment ΔT that ranges from $-3°$ to $9°C$. (An increase in ΔT results in increased sensitivity of density to temperature gradients.) The AMOC in these model integrations drops as the MDG increases regardless of whether the density difference is computed at the surface or averaged over the upper ocean. Traditional scaling analysis can only produce this weaker AMOC if the scale depth decreases enough to compensate for the stronger MDG. Five estimates of the depth scale are evaluated and it is found that the changes in the AMOC can be derived from scaling analysis when using the depth of the maximum overturning circulation or estimates thereof but not from the pycnocline depth. These two depth scales are commonly assumed to be the same in theoretical models of the AMOC. It is suggested that the correlation between the MDG and AMOC breaks down in these model integrations because the depth and strength of the AMOC is influenced strongly by remote forcing such as Southern Ocean winds and Antarctic Bottom Water formation.

1. Introduction

The idea that the Atlantic meridional overturning circulation (AMOC) is essentially a gravity-driven current system facilitated by a meridional density gradient (MDG) has a long history in physical oceanography and is recurrent in the climatological literature (Thorpe et al. 2001; Delworth and Dixon 2006; Straneo 2006). The connection between the AMOC and its MDG is often used in the diagnostics of model output and has been put forward as a motivation for studying the Southern Ocean (SO) when trying to establish AMOC states in the past (Hughes and Weaver 1994). Its most common application is that of the box model in which the flow is set to be proportional to the density difference between boxes (Stommel 1961; Rooth 1982; Marotzke 2000; Kahana et al. 2004; Oliver et al. 2005). While the

dynamics are physically correct for well-mixed, fixed-depth boxes in a nonrotating system, the real ocean dynamics are much more complicated than such an idealized system (Wunsch 2005). Nonetheless, because of its simplicity and intuitive appeal, the density-driven box model has been used widely to assess the stability of the thermohaline circulation in the present and in the past (Shaffer and Bendtsen 1994). The most famous of these studies is that of Stommel (1961) in which he predicted that the meridional circulation can have multiple steady states for the same boundary conditions. Bistability has since been reproduced in a multitude of 3D, rotating, multilayer ocean general circulation models, adding further credence to the density-driven overturning idea (Manabe and Stouffer 1988; Rahmstorf 1995; Prange et al. 2003; Marsh et al. 2004). It is still an open question whether the bistability is an artifact of the models' simplifying assumptions (Johnson et al. 2007; Nof et al. 2007). Note that a change in the meridional density gradient translates linearly to a change in the meridional density difference (MDD) as long as the meridional extent is constant. We assume here that the appropriate zonal boundaries are constant and thus shall use the terms interchangeably in this regard.

Theoretical arguments for a MDG-controlled overturning are usually based on the scaled thermal wind equations, together with the assumption that the zonal and meridional transports (or density gradients) are comparable. In basic form, the scaled equations actually predict an overturning driven by a scaled approximation of the meridional pressure gradients. When the further assumption is made that the vertical scale depth is constant, it is implied that the AMOC is linearly proportional to the MDG (details are presented in section 2). These scaling laws are supported by ocean general circulation models (GCMs) that exhibit a linear relationship between the maximum overturning streamfunction in the Atlantic and the MDG (Rahmstorf 1996; Thorpe et al. 2001; Griesel and Morales Maqueda 2006).

There is evidence, however, that this picture can change when the scaling depth for the overturning is not constant. For example, scaling analysis that incorporates the advective–diffusive balance leads to a ⅓ power scaling law (instead of a linear scaling law) between the AMOC and the MDD (Bryan 1987). Park (1999) found that using the nonlinear scaling resulted in a significantly more stable thermal mode in a two-box thermohaline circulation model. Moreover, a number of investigators have looked at cases where the turbulent dissipation in the pycnocline is constant so that the turbulent mixing coefficient is inversely proportional to the vertical density gradient (Munk and Wunsch 1998; Nilsson and Walin 2001; Watson and Naveira Garabato 2006; Guan and Huang 2008). Nilsson et al. (2003) showed that with such a representation of mixing the meridional overturning circulation can be anticorrelated to the surface MDG. However, it is not clear from their work whether their MOC is also anticorrelated with the MDG when the density gradient is averaged over the upper ocean (e.g., from the surface to the thermocline or the depth of maximum overturning), which is arguably a more appropriate value than the surface density gradient. Moreover, their model is a one-hemisphere sector model so that the vertical scale depth of the problem can only be controlled by local mixing and buoyancy forcing and not by remote forcing such as is present in the real ocean.

In this paper we present two sets of model integrations in which the scale height is not simply related to the MDG within the Atlantic. The studies described here, carried out using the Modular Ocean Model version 4 (MOM4), with an energy balance moisture transport atmosphere in an idealized global model with two ocean basins, allow for remote impacts on the scale depth of overturning. In one set of model integrations we allow the relative impacts of the temperature and salinity in the equation of state to change. In the experiments where temperature gradients become more important, the MOC in the Atlantic decreases in spite of a larger MDG. The pycnocline depth also increases but the depth of the maximum overturning is reduced owing to the influx of Antarctic Bottom Water. In the other set of model integrations, we change the wind stresses in the Southern Ocean. Again, even though the surface density gradient is reduced at large overturning rates in the Atlantic, the vertical scale depth increases to allow a stronger overturning.

This paper is organized as follows: section 2 describes the theoretical background to the density-overturning relation. The model description and experimental setup are explained in section 3 and the results discussed in section 4. Conclusions are drawn in section 5.

2. Theoretical background

Scaling analysis

The theoretical case for the MDG–AMOC relationship is based on the thermal wind equation (e.g., Cushman-Roisin 1994, 181–183). In scaled form it can be written as

$$UL = \frac{g\Delta\rho H}{\rho_o f_o},\tag{1}$$

where U is a typical zonal velocity, L is the length of the basin and $\Delta\rho$ the meridional density difference across the basin, H is the scale depth, ρ_o is a reference density, and f_o is a typical value for the Coriolis parameter. This

assumes that thermal wind balance holds on average over the entire region and depth range of interest; specifically, the velocity scale and the density difference apply over the depth scale H. To translate Eq. (1) into a meridional transport, the zonal velocity is assumed to be of similar magnitude to the meridional velocity V so that one can write the meridional transport above the scale depth as

$$\Psi = VLH = \frac{g\Delta\rho H^2}{\rho_o f_o}, \qquad (2)$$

where L is the width of the basin (assumed for simplicity to be equal to the length of the basin). In this form Eq. (2) represents a balance between the AMOC and the meridional pressure gradient (MPG). It is appropriate to point out that the assumption $U \sim V$ (or equivalently that $-\Delta\rho_x \sim \Delta\rho_y$) is not necessarily valid. Given that the basinwide velocities are to first order fixed by the wind stress through the Sverdrup transport, the meridional overturning circulation occurs through adjustments in the western boundary currents where $V \gg U$ (de Boer and Johnson 2007). In fact, one can envision a situation where all convection occurs in the Labrador Sea and none in the Greenland Sea so that the average U that is related to the overturning would be zero but the average V would not. However, support for the assumption is provided by Wright and Stocker (1991) in a steady-state, hemispheric basin simulation of the Bryan–Cox OGCM. They found good correlation between the zonal and meridional gradients of the vertically integrated density at 570-m and 2135-m depth.

Equation (2) has two unknown variables, $\Delta\rho$ and H, on its right-hand side. To secure a relation between Ψ and $\Delta\rho$ one needs to express H in terms of the remaining unknowns or obtain its value independently. In the simplest scenario, H is assumed to be constant. In this case the overturning transport is a linear function of the MDG,

$$\psi = \frac{gH_\rho^2}{\rho_0 f_0}\Delta\rho,$$

where H_ρ is a vertical scale such as the pycnocline depth and is assumed constant. In an ocean general circulation model, Rahmstorf (1996) found such a linear relationship between the overturning streamfunction in the Atlantic and the depth-integrated MDG between the 35°–40°S and 50°–55°N latitudinal bands. Thorpe et al. (2001) also found a linear relation when comparing the overturning to the steric height gradient. Note that, although they used the steric height instead of density, he integrated to a fixed depth H so that no account is taken of the variable depth of the overturning or thermocline and this makes it more relevant to the fixed H scaling above than to a scaling where the H is variable (as dis-

cussed below). The latter studies mentioned here (1994 and onward) used the tip of Africa as a southern boundary rather than the equator because it better represents the extent of the basin.

A second approach is to derive the scale depth H by assuming an advective–diffusive balance in the thermocline (Welander 1986; Bryan 1987). In scaled form the advective–diffusive balance can be written as

$$W = \frac{k_v}{H}, \qquad (3)$$

where K_v is the vertical diffusivity, and W is a typical vertical velocity that can be related to V through the incompressibility relation,

$$WL = VH. \qquad (4)$$

Equations (1)–(4) give

$$\psi = \left(\frac{gL^4 k_v^2}{\rho_0 f_0}\right)^{1/3}\Delta\rho^{1/3}. \qquad (5)$$

Under these assumptions, the overturning is proportional to the $\frac{1}{3}$ power of the MDG and to the $\frac{2}{3}$ power of the vertical diffusivity. Based on the above analysis, Park (1999) adapted the Stommel box model to use this $\frac{1}{3}$ power scaling of the overturning to the density gradient for the flow closure. Marotzke (1997) captured a $\frac{2}{3}$ power dependence of the overturning on vertical diffusivity in an idealized northern hemisphere basin-scale model where no wind forcing was applied and vertical mixing was nonzero only at the boundaries. For a discussion of numerical studies of this law see Park and Bryan (2000; and references therein).

In the above two approaches the scale depth was either assumed constant or derived from the advective–diffusive balance. Other closure schemes for H involve conservation of mass above the pycnocline (Gnanadesikan 1999) and considerations of energy conservation (Nilsson et al. 2003). Hughes and Weaver (1994) allowed for changes in the scale depth by integrating the density anomaly to the depth of the maximum in the meridional overturning streamfunction to determine the steric height in each run and found a linear relation between the overturning and the meridional steric height gradient. In this paper we investigate the validity of the assumption of a fixed proportionality (linear or to any positive power) between the AMOC and the MDG, as commonly used in box models.

3. Numerical study design

a. Description of the model

We perform a set of 15 model integrations in the MOM4 OGCM (Griffies et al. 2003) coupled to a sea ice

and energy moisture balance model. In one suite of seven model integrations the Southern Ocean winds south of 30°S were changed, and in a second suite of eight model integrations the equation of state was changed. Both the model setup and the experiment design for the simulations with a changed equation of state are described in detail in de Boer et al. (2007, 2008) where the model was used to investigate the response of the large-scale ocean circulation to mean ocean temperature change. The wind sensitivity model integrations are described in Gnanadesikan et al. (2007). For completeness, an overview of the model and experiments is provided here. The resolution of the ocean model is 4° latitude by 4° longitude and 24 layers in the vertical that range from 15 m at the surface and become progressively thicker toward the bottom at 5000-m depth. The ocean model has an idealized geometry, modeled after Bjornsson and Toggweiler (2001), in which the Indo-Pacific is represented by a rectangular box that has twice the width of the Atlantic box (Fig. 1). They are connected in the south by a circumpolar channel. Twenty-four ridges that are 2500 m deep, six grid points long, and one grid point wide are scattered evenly throughout the ocean to absorb the momentum of the Antarctic Circumpolar Current (ACC). The wind experiments were performed in a later version of the model in which the ridges were kept only in the ACC so that their control runs differ slightly. Horizontal tracer mixing and diffusion coefficients (Gent and McWilliams 1990; Redi 1982) are both set to 0.8×10^3 m^2 s^{-1}. Vertical diffusivity increases from 0.1×10^{-4} m^2 s^{-1} at the surface to 1.2×10^{-4} m^2 s^{-1} at depth. A zonal surface wind stress is applied, taken from an annual and zonal average of winds of the European Centre for Medium-Range Weather Forecasts (Trenberth et al. 1990). The equation of state, based on McDougall et al. (2003), is fully nonlinear and computes the in situ density and its partial derivatives with respect to potential temperature and salinity.

The atmospheric model is a one-layer two-dimensional (equivalent to 3° longitude by 2.25° latitude) spectral Energy Moisture Balance Model developed at the Geophysical Fluid Dynamics Laboratory (GFDL) (de Boer et al. 2007). It solves two prognostic equations for temperature and water vapor mixing ratio. Its temperature is determined by a balance of seasonal radiative fluxes at the top and bottom of the domain, lateral diffusion, and latent heat released when precipitation is formed. The mixing ratio depends on the evaporation from the ocean, precipitation, and lateral diffusion. The ocean and atmosphere are coupled by the GFDL Sea Ice Simulator (Winton 2000), an ice model that has the same horizontal resolution as the ocean and consists of two ice layers (of variable thickness) and one snow layer. A simple land
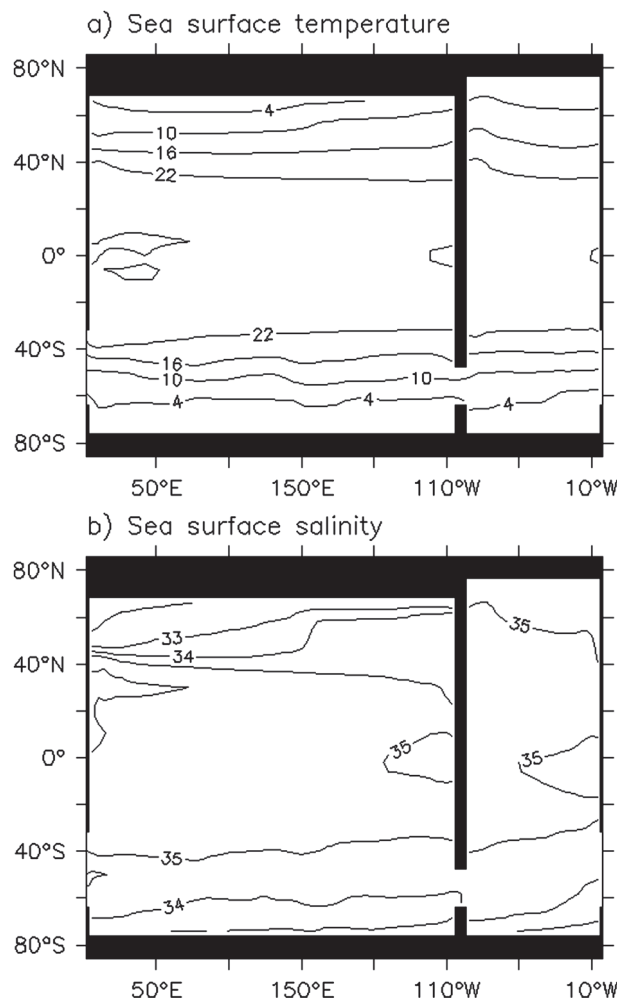

FIG. 1. Sea surface (a) temperature (°C) and (b) salinity in the control run of the EOS suite of model integrations.

model determines land surface temperatures according to a constant vegetation and soil type. Precipitation that falls on land runs off to the nearest ocean point. Each run is started from a horizontally homogenous initial temperature and salinity field and run out for 3000 years. At this time trends in all variables were weak and further integration is unlikely to change the conclusions drawn here. Result shown here are from data averaged over the last 10 years of each integration.

b. Experiment setup

The first set of model integrations [hereafter referred to as the wind stress (WS) suite] follows the experimental strategy of a line of research beginning with Toggweiler and Samuels (1993) in which winds are changed in the Southern Ocean but not elsewhere. In many of these previous simulations, however, the inclusion of salinity restoring at the ocean surface tightly

couples changes in Ekman-driven upwelling to changes in the surface water balance so that higher winds are always associated with greater freshening. Our model integrations use an energy balance model and, therefore, do not suffer from this unrealistic coupling. Six perturbation simulations are made from the baseline case in which the wind stress south of 30°S is multiplied by 0, 0.5, 0.75, 1.5, 2.0, and 3.0.

The second set of model integrations [hereafter referred to as the equation of state (EOS) suite] described here has differing integrations, not in parameter choice or boundary conditions, but in how the density is derived from the model temperature, salinity, and pressure. The real equation of state is nonlinear in temperature in the sense that temperature gradients result in stronger density gradients when the mean temperature is higher. (The nonlinearity w.r.t. salinity is less pronounced.) Here, the model density is evaluated, not at the model temperature T, but at $T + \delta T$ where δT takes on the value $-3°, -2°, 0°, 1.5°, 3°, 4.5°, 6°$, and $9°C$ in each of the eight model integrations, respectively. In other words, while the model temperature, T, is determined by the model dynamics and thermodynamics and never altered artificially, δT is added to the temperature when density or density gradients are calculated. We call this the dynamic density, $\rho_d = \rho(S, T + \delta T, p)$, where S is the salinity and p the pressure, to distinguish it from the tracer density, $\rho_t = \rho(S, T, p)$. The tracer density would result from a conventional application of the equation of state to the actual model temperature and salinity and is only used for diagnostic purposes. Note again that the adjustment to the temperature is only done in the calculation of the density and does not directly affect the temperature field and that the increment, δT, is spatially and temporally constant.

The EOS suite is uniquely suited to distinguish between the dynamical and passive tracer properties of temperature and salinity. While the model temperature responds to the circulation and heat fluxes the same way as in other models, the density (which influences the dynamics) has a different sensitivity to these fields. The cases where $\delta T > 0$ and $\delta T < 0$ are called the dynamically warm and dynamically cold case, respectively, to indicate that the mean temperature change only reflects on the dynamics of the system. It will be shown that there exists an *inverse* relationship between the MDG and the AMOC even though the tracer density gradient, derived from the actual temperature and salinity in the conventional way, scales linearly with the AMOC. Note that, although the seawater equation of state is not used in its usual sense here, the resulting density does not invalidate any of the dynamical equations used in the scaling or model equations.

c. Control run

In spite of the idealized geometry of the model, it captures the basic characteristics of the steady-state ocean circulation without the need of flux adjustments that are common in more realistic general circulation models. The coldest surface waters are found in the Southern Ocean, followed by the northwestern Pacific, and then the North Atlantic (Fig. 1a). The salinities of the surface polar waters are also realistic with the freshest waters occupying the North Pacific (Fig. 1b). The Antarctic waters are slightly more salty and the North Atlantic considerably more so due to the northward salt transport of the overturning circulation there. One obvious digression from observations is that the saltiest surface waters are found in our Indo-Pacific ocean basin, whereas in the real ocean they are in the subtropical Atlantic. For the EOS suite control run, the maximum meridional overturning streamfunction is 25 Sv (Sv $\equiv$ 10^6 m^3 s^{-1}) in the Atlantic and 5 Sv in the Pacific (Figs. 2a and 2b) and for the WS suite (with less bottom ridges) it is 25 Sv in the Atlantic and 6 Sv in the Pacific.

4. Results and discussion

a. Density and pressure scaling versus overturning

How does the overturning in these two suites depend on the surface density difference? We examine the maximum overturning in depth space and compare it to the density difference between the equator and the northernmost point in the "Atlantic" and "Pacific" basins. (Note that the scaling analysis for the AMOC–MDG relationship described in section 2 is based only on dynamic equations and not the conservation of heat so that, to test its validity, it is appropriate to use the dynamic density ρ_d for the EOS suite.) When overturning is compared with the surface density difference, we find that the AMOC is anticorrelated with the surface density difference in both the WS and EOS suites (Fig. 3a). In the Pacific there is no evident relationship in the WS suite, but a positive correlation in the EOS suite. When an average is taken over the top 1400 m, the AMOC remains anticorrelated to the Atlantic MDG in the EOS suite and is very poorly related to the overturning in the WS suite (Fig. 3b), though the overturning in the Pacific is now correlated with the MDG in both suites.

The EOS suite is the first study to our knowledge that has found an inverse relationship between the depth-integrated MDG and the AMOC. How robust is the anticorrelation? As shown in Fig. 4, taking shallower or deeper levels does not change the relationship. Changing the southern endpoint of the MDG from the equator to 30°S [as done by Hughes and Weaver (1994) and
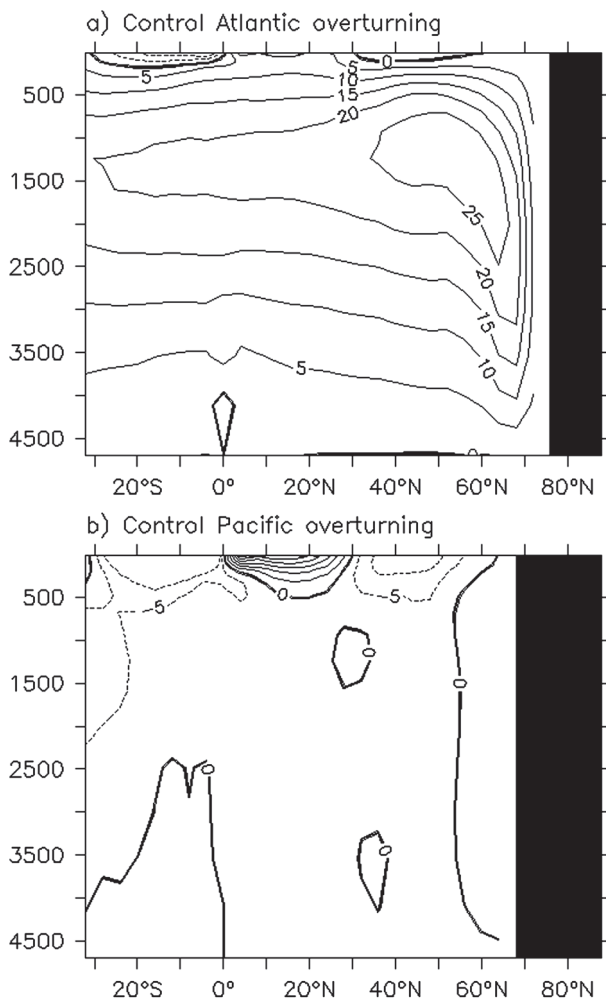
FIG. 2. The meridional overturning streamfunction in the (a) Atlantic and (b) Pacific for the control run of the EOS suite of model integrations.

Rahmstorf (1996)] does not affect the inverse relationship between the AMOC and MDG either (Fig. 4). Thorpe et al. (2001) used the meridional steric height gradient integrated to a fixed depth of 3000 m instead of the MDG. For our model integrations, the meridional steric height gradient was also determined (not shown here) and, similarly to the MDG, found to be anticorrelated to the AMOC in the EOS suite irrespective of the specific depth or latitudes taken. The meridional steric height gradient was calculated by twice vertically integrating the specific density anomaly to a fixed depth.

Is the lack of correlation between the MDG and the MOC due to a disconnect between the zonal and meridional pressure gradients or between the pressure and the density gradients? As shown in Fig. 5, the answer appears to be that the meridional pressure gradient is a good indicator of the overturning so that the disconnect
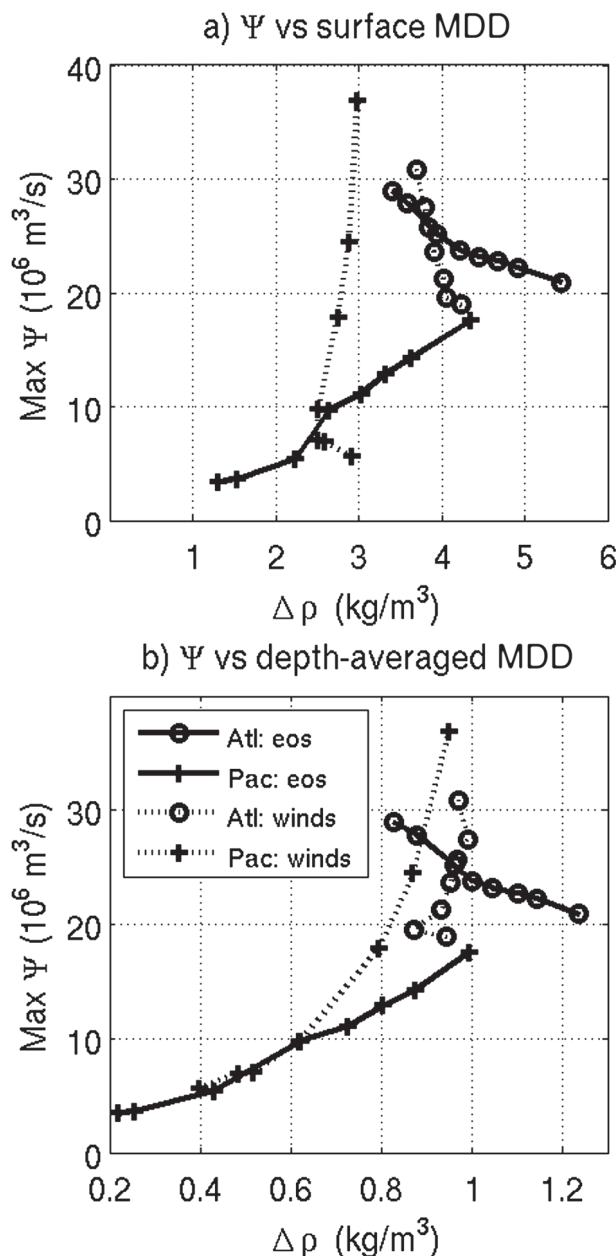

FIG. 3. The maximum overturning streamfunction Ψ in the Atlantic (circles) and the Pacific (crosses) as a function of the meridional density gradient (a) at the surface and (b) averaged from 0 to 1400 m between the equator and the northernmost grid point (66°N in Pacific and 74°N in Atlantic). For the EOS suite (solid lines) points on each line from left to right indicate the eight model integrations of $\Delta T = -3°, -2°, 0°, 1.5°, 3°, 4.5°, 6°,$ and 9°C, respectively. The WS suite (dotted lines) points on each line from bottom to top (increasing in Ψ) correspond to winds in the Southern Ocean multiplied by a factor of 0, 0.5, 0.75, 1, 1.5, 2, and 3, respectively. At the surface, the density gradient is anticorrelated with the Atlantic MOC in both studies and this relation persists when the density gradient is evaluated over the top 1400 m for the equation of state set. The Pacific overturning increases with stronger MDD in all cases except surface MDD of the very low SO winds model integrations.
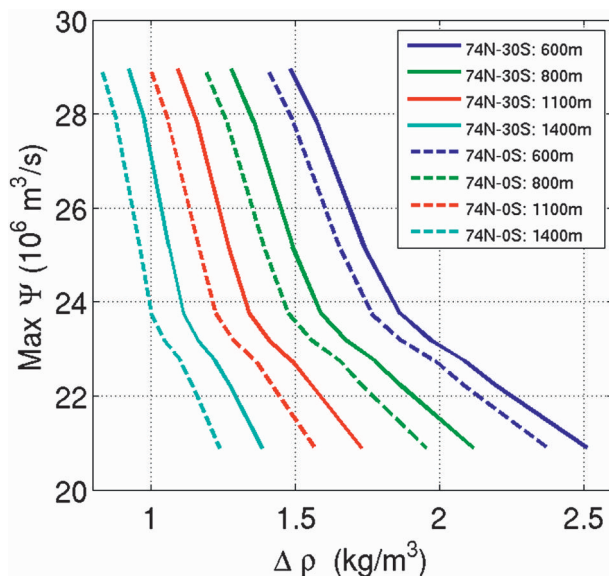
FIG. 4. The maximum overturning streamfunction Ψ in the Atlantic as a function of the meridional density difference between 74°N and 30°S (solid line) and the equator (dashed line) for the EOS suite. The density is vertically averaged from the surface to 600 m (dark blue), 800 m (green), 1100 m (red), and 1400 m (light blue), respectively. The inverse relationship between the AMOC and the MDD holds in all cases.
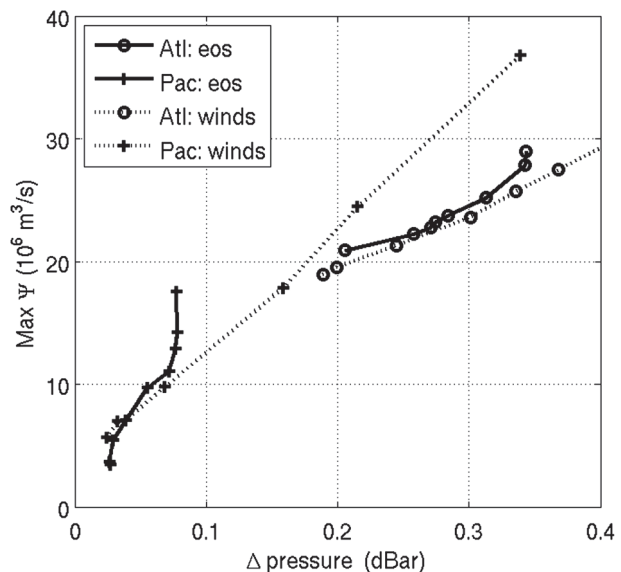

FIG. 5. Relationship between maximum overturning streamfunction and the pressure difference between the equator and northernmost grid points in the Atlantic (circles) and the Pacific (crosses) for the changed equation of state (solid lines) and the SO winds (dotted lines) suites. The pressure is averaged from 0 to 1400 m and given in units of decibars. In both basins for both suites the relation between the AMOC and the MPG is close to linear.

is rather between the MDG and the MPG. The average meridional pressure difference between 0 and 1400 m correlates much better with the overturning than the density difference. The stratification that leads to a reduced MDG, yet an increased MPG and overturning, is illustrated in Fig. 6a. Here profiles are shown of the density differences in the Atlantic western boundary between 74°N and the equator for the two extreme cases of the EOS suite. In the surface and upper layer the north–south density difference is lower for the high overturning run. However, the curvature of the density profile adapts so that the meridional pressure difference is higher in the upper ocean and the depth at which the pressure difference changes sign is deeper (Fig. 6b). These results raise several questions. First, what is the linkage between meridional density differences and pressure gradients? Second, to what extent is the classical result linking higher density gradients to higher overturning primarily a consequence of the responsive behavior of temperature and salinity to a higher MOC? Finally, what process leads to the inverse AMOC–MDG relation observed here?

b. Linking the density gradient and the pressure gradient

It is clear from our work that no universal scaling law exists that can link the AMOC and the MDG with a

fixed positive proportionality constant. However, it remains an open question whether the scaling of Eq. (2) is valid for a variable depth scale that is not assumed to be fixed or set by the vertical diffusivity. In other words, is it possible to define a depth scale H so that the AMOC is always positively correlated to $\Delta\rho H^2$ even when the AMOC is not positively correlated to the MDG? We shall consider five possible estimates for H and determine how well they capture the overturning in these two suites of experiments.

Traditionally the appropriate depth scale has been assumed to be the depth of the pycnocline (Gnanadesikan 1999; Park 1999; Nilsson et al. 2003). Usually the assumption is made that it is also the depth over which the northward transport occurs because the meridional velocity is integrated over this depth to give an estimate of the transport. The pycnocline depth can be estimated from the vertical density distribution at midlatitudes, and we evaluate two methods to do so. The first pycnocline depth approximation is that of Nilsson et al. (2003) in which

$$H = \int_{-D}^{0} \frac{\rho - \rho_D}{\rho_0 - \rho_D}\, dz, \qquad (6)$$

where ρ is the density at z, ρ_0 is the surface density, and ρ_D is the density at the bottom (depth D). The scale depth, H, is then averaged zonally across the width of
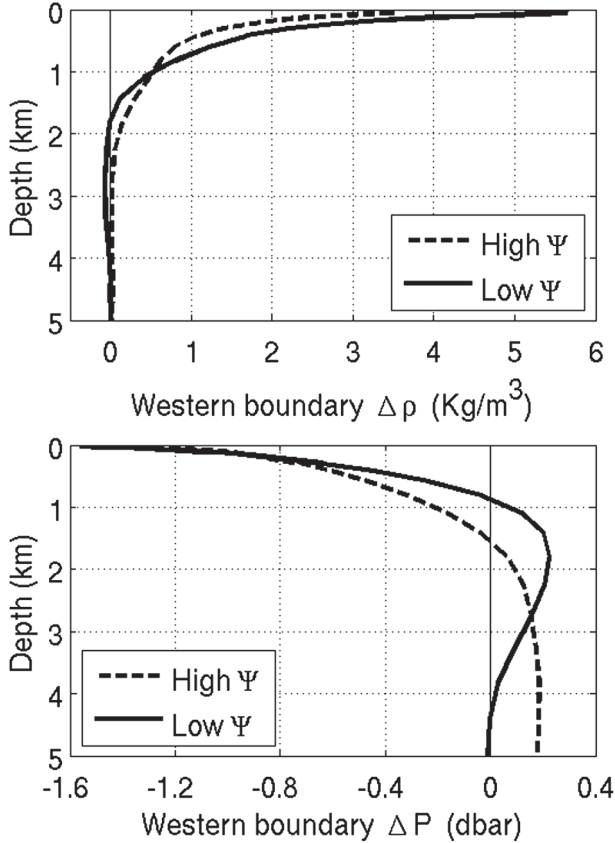
FIG. 6. Atlantic western boundary (top) meridional density difference and (bottom) pressure difference in the EOS suite. The difference is taken between 74°N and the equator and shown here for the highest overturning case where $\delta T = -3$°C (dashed lines) and for the lowest overturning case where $\delta T = 9$°C (straight lines). The case for high overturning corresponds to a weaker meridional density difference in the western boundary, but a stronger negative pressure difference in the upper part of the ocean that changes sign at a deeper level.
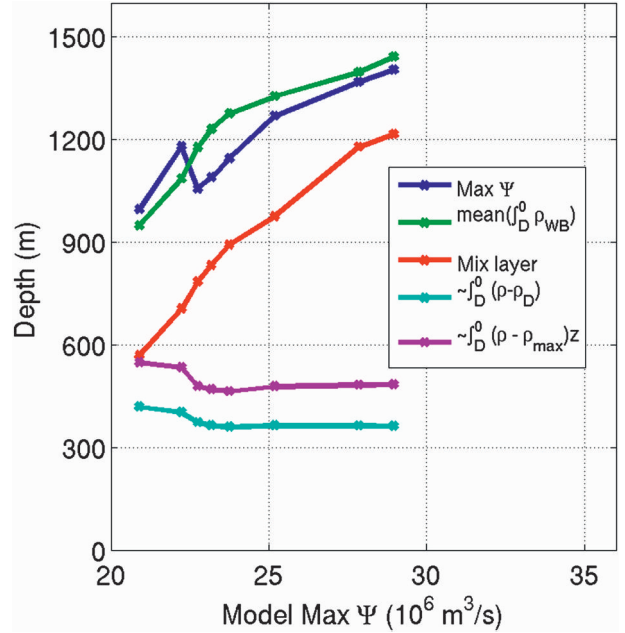
FIG. 7. The five estimates discussed in the text of the scale depth shown as a function of the maximum Atlantic overturning streamfunction for the EOS suite. The depth of the maximum overturning streamfunction (black), the depth of the mean of the depth-integrated meridional density gradient in the western boundary from Eq. (8) (blue), and the average mixed layer depth between 68° and 76°N in the Atlantic (pink) all show an increase with overturning. The pycnoline depth derived from Eq. (6) (green) and Eq. (7) (red) both show a slight decrease with the overturning.

the basin and from 30°S to 30°N. Nilsson et al. (2003) evaluated H at 30°N. We choose the wider area average as being more representative of the thermocline but have confirmed that evaluating H at 30°N does not affect our conclusions. The second method is that of Gnanadesikan (1999) and here the density is depth weighted so that

$$H = \frac{\int_{-D}^{0} z(\rho - \rho_{max})\, dz}{\int_{-D}^{0} (\rho - \rho_{max})\, dz}, \qquad (7)$$

where ρ_{max} is the maximum density and H is averaged horizontally as above. In the EOS suite, the pycnocline derived from both these methods shallows with increasing overturning in the Atlantic basin (Fig. 7). It is clear that H obtained from either Eq. (6) or (7) is not

a good approximation for the scale depth. In order for the overturning to scale with $\Delta \rho H^2$ for the EOS suite, the scale depth needs to increase with the overturning because $\Delta \rho$ and the overturning are anticorrelated.

An arguably more appropriate scale depth is the depth of the maximum of the overturning streamfunction as this is also the depth to which the meridional velocity must be integrated to get the northward transport in the derivation of Eq. (2). This depth does indeed increase with increased overturning (Fig. 7). Scaling analysis is often most useful when the full velocity field is not available and we would like, therefore, to find an estimate of the depth of the overturning that can be derived from more limited information. We focus on the western boundary because the interior transport is dominated by the wind field and changes in the overturning circulation are largely facilitated by western boundary currents. Moreover, the deepening of the overturning streamfunction is evident in the north–south pressure difference in the western boundary (Fig. 6). Usually the pressure field is not available from observations, but an estimate of the pressure difference in the western boundary can be derived by depth integrating the density difference (between 74°N and the equator) and setting the integration constant such that the average

north–south pressure gradient is zero. More precisely, the depth so obtained is where the depth-integrated density is equal to the vertical mean of the depth-integrated density so that

$$\int_H^0 \Delta\rho \, dz = \int_D^0 \int \Delta\rho \, dz' \, dz/D. \qquad (8)$$

This estimate of H also increases with the overturning strength and reproduces the depth of the maximum overturning streamfunction very well (Fig. 7).

The last estimate of the scale depth that we consider is that of Spall and Pickart (2001) who derived theoretically an estimate of the overturning for which the scale depth is the mixed layer depth at the northern boundary of the basin where the convection occurs. (They do not substitute the meridional for the zonal density difference, but rather use the zonal density difference across the northern boundary. Because we are investigating a derivation for the meridional pressure gradient here, we will only consider their depth scale.) To estimate the mixed layer depth we have averaged the annual mixed layer depth across the Atlantic in the two northernmost grid points. The mixed layer depth also increases linearly with the strength of the overturning (Fig. 7). It may seem obvious at first that the mixed layer depth will be deeper for a strong overturning but previous works have suggested that the link between the overturning strength and the convection is not straightforward (Marotzke and Scott 1999).

Of the five estimates of the scale depth considered here, only the last three, which are related to the depth of the maximum overturning circulation, can reasonably predict the overturning from Eq. (2). We evaluate the scaled estimate for the overturning from Eq. (2) for each of these three scale depths for the Atlantic and Pacific and for the EOS and WS suites. For each of the four sets of Ψ estimates (two basins and two suites) the estimated overturning is normalized so that the average estimate is equal to the average of the model maximum overturning streamfunction. (We are not interested in the proportionality constant between Ψ and $\Delta\rho H^2$ but rather in whether it is linearly proportional.) The meridional density difference, $\Delta\rho$, is taken as the zonal average of the difference between the density at the northern boundary and the equator and averaged from the surface to 1400-m depth. The best overall fit is obtained from Eq. (8) where H is assumed as the depth where the derived meridional pressure gradient in the western boundary is zero (Fig. 8). In this case the average absolute difference between the estimated overturning and the model overturning for the two basins and the 15 model integrations is 1.7 Sv, compared to 1.8 Sv where H is the maximum depth of the overturning, and 3.1 Sv
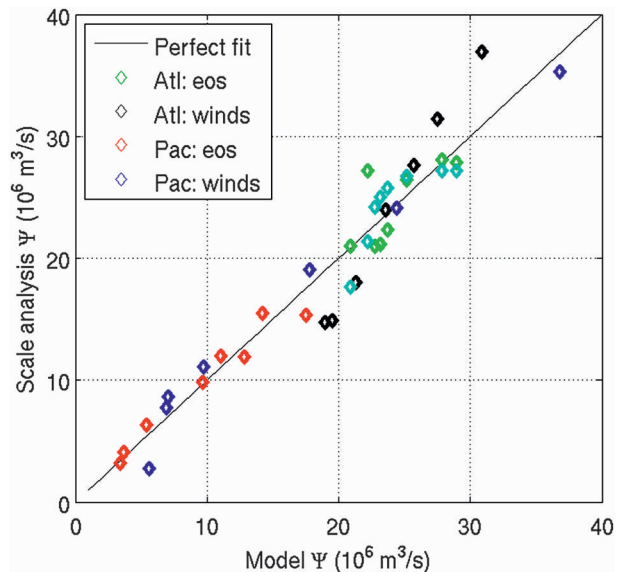

FIG. 8. Estimates of the maximum Ψ from scaling analyses [Eq. (2)] using the depth of the mean western boundary depth-integrated density gradient as the scale depth [Eq. (8)] and the 0–1400 m depth-averaged MDD between the equator and the northern most gridpoint (66°N in Pacific and 74°N in Atlantic). The EOS model integrations are shown in green (Atlantic) and red (Pacific) diamonds and the WS model integrations are shown in black (Atlantic) and blue (Pacific) diamonds. Estimates for each of the four groups are normalized so that their average Ψ is equal to the average Ψ of the model.

where H is the mixed layer depth. (Note that, owing to the normalization, the differences are more a measure of the skill of the scaling analysis to capture variability of the overturning as a function of $\Delta\rho H^2$ than of its skill to predict the absolute overturning.)

c. Is the classic correlation between MDG and AMOC accidental or fundamental?

The inverse proportionality between the AMOC and depth-averaged MDG found in the EOS suite is in contrast to previous numerical model experiments in the literature. Such experiments have found a positive correlation between the AMOC and MDG, apparently validating all of the assumptions inherent in the scaling arguments of section 2. Alternatively, it is possible that a stronger overturning circulation leads to a stronger density gradient purely because of its effect on temperature and salinity as tracers and not because a stronger density gradient is essential to set up the stronger zonal pressure gradient that is needed for a stronger AMOC. In the EOS suite the overturning is forced to change without any alterations to the surface fluxes, diffusivities, or wind field, and as a consequence the temperature and salinity adjustments that occur are due to the circulation only (and of course through the
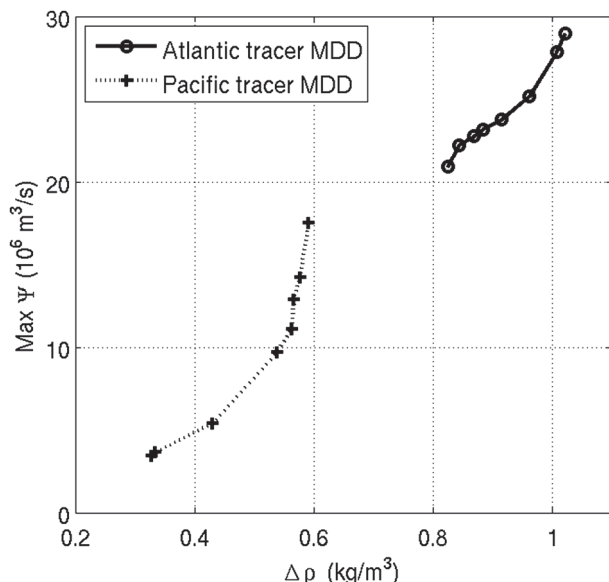
FIG. 9. The maximum overturning streamfunction Ψ for the EOS suite in the Atlantic (solid line) and the Pacific (dashed–dotted line) as a function of the meridional density gradient averaged from 0 to 1400 m between the equator and the northernmost grid point (66°N in Pacific and 74°N in Atlantic). Here the tracer density is used to calculate the MDD. In other words, the density is evaluated at the actual model temperature and salinity and not at the $T + \delta T$ used in the model. This tracer density is used for diagnostic purposes only. Now both the Pacific and Atlantic overturning exhibit a positive correlation between the MDD and the maximum overturning streamfunction.
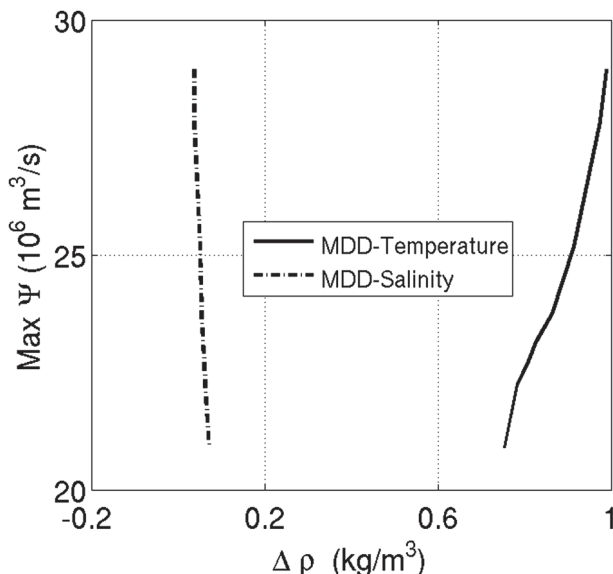

FIG. 10. The change in Atlantic maximum overturning as a function of changes in the tracer MDD (for the EOS suite). The effects of tracer temperature on the MDD (solid line) and salinity on the MDD (dashed line) are separated to distinguish them. As in previous figures, the density is vertically integrated from the surface to 1400 m and the gradient taken between the equator and 74°N. The increase in the tracer MDD with stronger AMOC found in Fig. 9 is due to an increase in the meridional temperature gradient. Changes in the salinity gradient are much smaller and of opposite sign.

secondary feedback effect of the temperature and circulation changes on the surface fluxes). It is therefore of interest to see what the MDG associated with the model temperature and salinity would have been if it was calculated from the seawater equation of state without the added increment δT. Figure 9 shows that the AMOC scales linearly with this tracer MDG, supporting the view that a stronger AMOC affects the temperature and salinity fields in such a way that they exhibit a stronger density gradient, but that this gradient is not a prerequisite for a stronger AMOC.

It is not feasible to examine all previous studies to determine what the causes in each case are for the stronger MDG when the AMOC is stronger, but we can examine this here. Figure 10 shows that the increase in the tracer density gradient at higher dynamic temperatures is due to an increase in the meridional temperature gradient, ΔT_m. The change in density that is due to salinity is seven times smaller and of the wrong sign to explain the observed trend. In fact, there is almost no salinity gradient because the Antarctic Intermediate Water equivalent in this model tends to freshen the subsurface equatorial waters. The tracer MDG trends are

thus further examined by zonally averaging the temperature field in the Atlantic and subtracting the strong AMOC, $T - 3°C$ case, from the weak AMOC, $T + 9°C$ case (Fig. 11). The first striking aspect is that almost the entire ocean is colder in the case where density is calculated at higher temperatures. The reason is that, in this dynamically warm case, the sinking in the Southern Ocean is dramatically increased and as a result the ocean is ventilated by cold Southern Ocean water instead of warmer North Atlantic waters (de Boer et al. 2007). In the surface ocean (roughly the top 100 m), ΔT_m is stronger in the dynamically warm case (weak AMOC), as one would expect from a weaker overturning that transports less heat northward and thus leaves the North Atlantic colder. Below the surface layer ΔT_m evolves in the opposite sense. The low-latitude deep ocean is more ventilated by cold Southern Ocean water due to the shoaling of the AMOC cell and the increase in Southern Ocean deep-water formation, leading to a reduced tracer MDG. This explanation clearly pertains only to the EOS suite, but it is possible that similar mechanisms apply to lead to a positive AMOC–MDG relation when the ocean circulation is perturbed in other ways (e.g., increased mixing or altered surface fluxes).
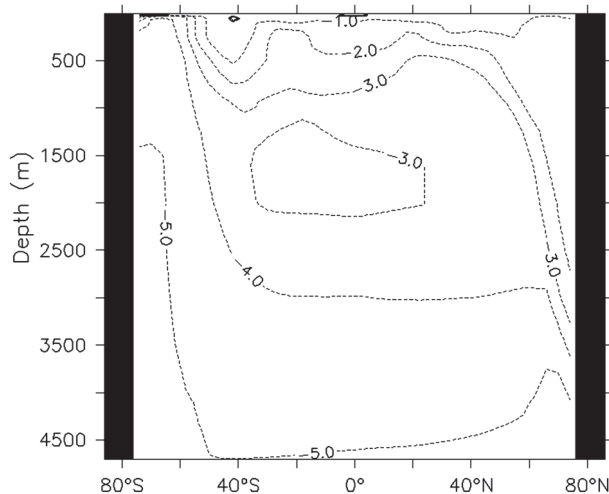
FIG. 11. Zonally averaged Atlantic temperature difference between the dynamically warm case ($\delta T = 9°C$, weak AMOC) and the dynamically cold case ($\delta T = -3°C$, strong AMOC). The ocean is colder in the dynamically warm case because it is more ventilated by water from the Southern Ocean. The temperature gradient is weaker in the dynamically warm case; the subsurface equatorial water cools more due to SO ventilation than the subsurface water in the North Atlantic where deep water is formed at a higher temperature than in the SO.

d. What process is responsible for the inverse AMOC–MDG relation in the EOS suite?

In the EOS suite, the tracer MDG is proportional to the AMOC even though the dynamic MDG used in the model dynamics is not. Thus, a smaller overturning at higher temperature corresponds to a smaller temperature difference ΔT_m but a larger density difference $\delta\rho/\delta T \times \Delta T_m$. The increase in density gradient is thus driven by the coefficient of thermal expansion increasing with temperature. However, such an explanation is not complete. Indeed, why does ΔT_m not just decrease more so as to compensate for the increase in $\delta\rho/\delta T$ and thus give the positively correlated MDG–AMOC relation that is so common in other studies? We suggest that the reason why these model integrations behave at odds with previous studies is that the AMOC is not changed by its local forcing but responds mainly to the changes occurring in the Southern Ocean. De Boer et al. (2007) showed that, when the dynamic temperature is high in these model integrations, the North Atlantic, Southern Ocean, and North Pacific all become less stable during their respective winter seasons. One would expect the North Atlantic to produce more deep water when its vertical stratification is less stable. But, what we find is that it produces less deep water while the Southern Ocean produces significantly more. Even though the general stratification in the Atlantic leans more toward a stronger AMOC, the strong source of Southern Ocean deep water does not allow for

it to increase. Supplementary work (not shown here) confirms that in an ensemble of model integrations of the Genie Goldstein ocean model (Edwards et al. 1998), the AMOC–MDG relation can break down when both the Southern Ocean and North Atlantic become less stable but the Southern Ocean more so than the North Atlantic. In such a case, even though the MDG in the Atlantic is stronger, the increase in Southern Ocean deep-water formation prevents an increase in North Atlantic deep-water formation and reduces the vertical scale depth of the Atlantic MOC.

5. Conclusions

Two suites of model integrations have been produced in which the AMOC is negatively correlated to the surface MDG in the Atlantic. In the suite with a changed equation of state, this anticorrelation persists when an average is taken over the upper ocean. This illustrates quite clearly that strong local density gradients are not in themselves indicative of a strong AMOC. It is suggested that the proportionality between the AMOC and MDG, common in numerical model studies, is largely a feedback of the circulation as opposed to a necessary condition. The MDG does contribute directly to the meridional pressure gradients and these do predict the overturning well in all our model integrations in both the Atlantic and Pacific. However, the vertical stratification determines how these density gradients are converted to pressure gradients. In scaling analysis of the overturning circulation, the vertical stratification is represented by the scale depth. Scaling estimates of the overturning based on five options for the scale depth of the overturning are derived. Similar to Griesel and Morales Maqueda (2006), the pycnocline depth is relatively unresponsive to changes in the meridional circulation, and we find that it does not capture the depth structure of the overturning well. We argue that a more appropriate estimate of the scale depth is the depth of the maximum overturning streamfunction. The best estimate of the overturning is obtained when the depth scale is taken to be the depth where the derived meridional pressure gradient in the western boundary is zero. It is an interesting outcome of this work that the pycnocline depth and the depth of maximum overturning does not necessarily respond in the same way (i.e., with the same sign) to outside forcing. Most theoretical models of the overturning assume that these scale depths are the same (Gnanadesikan 1999; Nilsson and Walin 2001; Johnson et al. 2007).

Our results indicate that a necessary (but not sufficient) condition for a decrease in overturning in spite of a stronger MDG is that the depth over which the northward transport occurs must decrease. If the North

Atlantic overturning is forced locally to decrease (e.g., through changes in the North Atlantic freshwater flux or increased vertical diffusivity in a sector model), then the depth of overturning will decrease as well as the MDG. We argue that, in order to reduce the overturning but not the MDG, the depth of the overturning must be forced to decrease through an influx of Southern Ocean or North Pacific water that is remotely forced. In such circumstances the overturning in the Atlantic can be reduced even when the upper-layer density gradient is stronger. In both suites here, changes remote from the North Atlantic—either the Southern Ocean wind stress or bottom-water formation in the Southern Ocean—act to change the scale depth of the overturning in ways that are far more important than the density gradient.

The results in this paper, that is, that the AMOC is not necessarily positively correlated with the MDG, warn against putting too much faith in conclusions drawn from density-driven box models because they operate under this dynamic regime. One may be tempted to argue that the dependence of the circulation in such box models on the MDG is correct because it is based on a fixed correspondence between the MDG and the MPG and that model studies, so far, all show a positive correlation between the AMOC and the MPG. This may be true for these box models, but the assumptions rely on the inherent property of box models that the scale depth is fixed, and we have shown that this is not the case in the real ocean and can be of fundamental importance. The inclusion of wind forcing is an important generalization of box models, but even where wind is included the assumption of a fixed relation between the MOC and MDG can break down if the scale depth remains fixed. Fixed-depth, density-driven box models may only be appropriate for studies of the AMOC in which deep-water formation in the Southern Ocean and North Pacific is not expected to change.

REFERENCES

Bjornsson, H., and J. R. Toggweiler, 2001: The climatic influence of Drake Passage. *The Oceans and Rapid Climate Change: Past, Present, and Future, Geophys. Monogr.,* Vol. 126, Amer. Geophys. Union, 243–259.

Bryan, F., 1987: Parameter sensitivity of primitive equation ocean general circulation models. *J. Phys. Oceanogr.,* **17,** 970–985.

Cushman-Roisin, B., 1994: *Introduction to Geophysical Fluid Dynamics.* Prentice Hall, 320 pp.

de Boer, A. M., and H. L. Johnson, 2007: Inferring the zonal distribution of measured changes in the meridional overturning circulation. *Ocean Sci.,* **3,** 55–57.

——, D. M. Sigman, J. R. Toggweiler, and J. L. Russell, 2007: Effect of global ocean temperature change on deep ocean ventilation. *Paleoceanography,* **22,** PA2210, doi:10.1029/2005PA001242.

——, J. R. Toggweiler, and D. M. Sigman, 2008: Atlantic dominance of the meridional overturning circulation. *J. Phys. Oceanogr.,* **38,** 435–450.

Delworth, T. L., and K. W. Dixon, 2006: Have anthropogenic aerosols delayed a greenhouse gas-induced weakening of the North Atlantic thermohaline circulation? *Geophys. Res. Lett.,* **33,** L02606, doi:10.1029/2005GL024980.

Edwards, N. R., A. J. Willmott, and P. D. Killworth, 1998: On the role of topography and wind stress on the stability of the thermohaline circulation. *J. Phys. Oceanogr.,* **28,** 756–778.

Gent, P. R., and J. C. McWilliams, 1990: Isopycnal mixing in ocean circulation models. *J. Phys. Oceanogr.,* **20,** 150–155.

Gnanadesikan, A., 1999: A simple predictive model for the structure of the oceanic pycnocline. *Science,* **283,** 2077–2079.

——, A. M. de Boer, and B. K. Mignone, 2007: A simple theory of the pycnocline and overturning revisited. *Ocean Circulation: Mechanisms and Impacts, Geophys. Monogr.,* Vol. 173, Amer. Geophys. Union, 19–32.

Griesel, A., and M. A. Morales Maqueda, 2006: The relation of meridional pressure gradients to North Atlantic deep water volume transport in an ocean general circulation model. *Climate Dyn.,* **26,** 781–799.

Griffies, S. M., M. J. Harrison, R. C. Pacanowski, and A. Rosati, 2003: A technical guide to MOM4. NOAA/Geophysical Fluid Dynamics Laboratory Ocean Group Tech. Rep. No. 5, 342 pp. [Available online at http://www.gfdl.noaa.gov/bibliography/related_files/smg0301.pdf.]

Guan, Y. P., and R. X. Huang, 2008: Stommel's box model of thermohaline circulation revisited—The role of mechanical energy supporting mixing and the wind-driven gyration. *J. Phys. Oceanogr.,* **38,** 909–917.

Hughes, T. M. C., and A. J. Weaver, 1994: Multiple equilibria of an Asymmetric 2-Basin Ocean Model. *J. Phys. Oceanogr.,* **24,** 619–637.

Johnson, H. L., D. P. Marshall, and D. A. J. Sprowson, 2007: Reconciling theories of a mechanically driven meridional overturning circulation with thermohaline forcing and multiple equilibria. *Climate Dyn.,* **29,** 821–836.

Kahana, R., G. R. Bigg, and M. R. Wadley, 2004: Global ocean circulation modes derived from a multiple box model. *J. Phys. Oceanogr.,* **34,** 1811–1823.

Manabe, S., and R. J. Stouffer, 1988: Two stable equilibria of a coupled ocean-atmosphere model. *J. Climate,* **1,** 841–866.

Marotzke, J., 1997: Boundary mixing and the dynamics of three-dimensional thermohaline circulations. *J. Phys. Oceanogr.,* **27,** 1713–1728.

——, 2000: Abrupt climate change and thermohaline circulation: Mechanisms and predictability. *Proc. Natl. Acad. Sci. USA,* **97,** 1347–1350.

——, and J. R. Scott, 1999: Convective mixing and the thermohaline circulation. *J. Phys. Oceanogr.,* **29,** 2962–2970.

Marsh, R., and Coauthors, 2004: Bistability of the thermohaline circulation identified through comprehensive 2-parameter sweeps of an efficient climate model. *Climate Dyn.,* **23,** 761–777.

McDougall, T. J., D. R. Jackett, D. G. Wright, and R. Feistel, 2003: Accurate and computationally efficient algorithms for potential

temperature and density of seawater. *J. Atmos. Oceanic Technol.,* **20,** 730–741.

Munk, W., and C. Wunsch, 1998: Abyssal recipes II: Energetics of tidal and wind mixing. *Deep-Sea Res.,* **45,** 1977–2010.

Nilsson, J., and G. Walin, 2001: Freshwater forcing as a booster of thermohaline circulation. *Tellus,* **53A,** 629–641.

——, G. Brostrom, and G. Walin, 2003: The thermohaline circulation and vertical mixing: Does weaker density stratification give stronger overturning? *J. Phys. Oceanogr.,* **33,** 2781–2795.

Nof, D., S. Van Gorder, and A. de Boer, 2007: Does the Atlantic meridional overturning cell really have more than one stable steady state? *Deep-Sea Res. I,* **54,** 2005–2021.

Oliver, K. I. C., A. J. Watson, and D. P. Stevens, 2005: Can limited ocean mixing buffer rapid climate change? *Tellus,* **57A,** 676–690.

Park, Y. G., 1999: The stability of thermohaline circulation in a two-box model. *J. Phys. Oceanogr.,* **29,** 3101–3110.

——, and K. Bryan, 2000: Comparison of thermally driven circulations from a depth-coordinate model and an isopycnal-layer model. Part I: Scaling-law sensitivity to vertical diffusivity. *J. Phys. Oceanogr.,* **30,** 590–605.

Prange, M., G. Lohmann, and A. Paul, 2003: Influence of vertical mixing on the thermohaline hysterises: Analyses of an OGCM. *J. Phys. Oceanogr.,* **33,** 1707–1721.

Rahmstorf, S., 1995: Bifurcations of the Atlantic Thermohaline Circulation in response to changes in the hydrological cycle. *Nature,* **378,** 145–149.

——, 1996: On the freshwater forcing and transport of the Atlantic thermohaline circulation. *Climate Dyn.,* **12,** 799–811.

Redi, M. H., 1982: Oceanic isopycnal mixing by coordinate rotation. *J. Phys. Oceanogr.,* **12,** 1154–1158.

Rooth, C., 1982: Hydrology and ocean circulation. *Prog. Oceanogr.,* **11,** 131–149.

Shaffer, G., and J. Bendtsen, 1994: Role of the Bering Strait in controlling North-Atlantic Ocean circulation and climate. *Nature,* **367,** 354–357.

Spall, M. A., and R. S. Pickart, 2001: Where does dense water sink? A subpolar gyre example. *J. Phys. Oceanogr.,* **31,** 810–825.

Stommel, H., 1961: Thermohaline convection with 2 stable regimes of flow. *Tellus,* **13,** 224–230.

Straneo, F., 2006: On the connection between dense water formation, overturning, and poleward heat transport in a convective basin. *J. Phys. Oceanogr.,* **36,** 1822–1840.

Thorpe, R. B., J. M. Gregory, T. C. Johns, R. A. Wood, and J. F. B. Mitchell, 2001: Mechanisms determining the Atlantic thermohaline circulation response to greenhouse gas forcing in a non-flux-adjusted coupled climate model. *J. Climate,* **14,** 3102–3116.

Toggweiler, J. R., and B. Samuels, 1993: Is the magnitude of the deep outflow from the Atlantic Ocean actually governed by Southern Hemisphere winds? *The Global Carbon Cycle,* M. Heimann, Ed., NATO ASI Series, Vol. I15, Springer-Verlag, 303–331.

Trenberth, K. E., W. G. Large, and J. G. Olson, 1990: The mean annual cycle in global ocean wind stress. *J. Phys. Oceanogr.,* **20,** 1742–1760.

Watson, A. J., and A. C. Naveira Garabato, 2006: The role of Southern Ocean mixing and upwelling in glacial–interglacial atmospheric CO$_2$ change. *Tellus,* **58B,** 73–87.

Welander, P., 1986: Thermohaline effects in the ocean circulation and related simple models. *Large-Scale Transport Processes in Oceans and Atmosphere,* J. Willebrand and D. L. T. Anderson, Eds., D. Reidel, 163–200.

Winton, M., 2000: A reformulated three-layer sea ice model. *J. Atmos. Oceanic Technol.,* **17,** 525–531.

Wright, D. G., and T. F. Stocker, 1991: A zonally averaged ocean model for the thermohaline circulation. 1. Model development and flow dynamics. *J. Phys. Oceanogr.,* **21,** 1713–1724.

Wunsch, C., 2005: Thermohaline loops, Stommel box models, and the Sandstrom theorem. *Tellus,* **57A,** 84–99.